# New Journal of Physics

The open access journal at the forefront of physics

CrossMark

**PAPER**

# Dynamics of distorted skyrmions in strained chiral magnets

J Chen[1,2], J J Liang[1], J H Yu[1], M H Qin[1,4], Z Fan[1], M Zeng[1] ⓘ, X B Lu[1], X S Gao[1], S Dong[2,4] ⓘ and J-M Liu[3]

1  Institute for Advanced Materials, South China Academy of Advanced Optoelectronics and Guangdong Provincial Key Laboratory of Quantum Engineering and Quantum Materials, South China Normal University, Guangzhou 510006, People's Republic of China
2  School of Physics, Southeast University, Nanjing 211189, People's Republic of China
3  Laboratory of Solid State Microstructures, Nanjing University, Nanjing 210093, People's Republic of China
4  Author to whom any correspondence should be addressed.

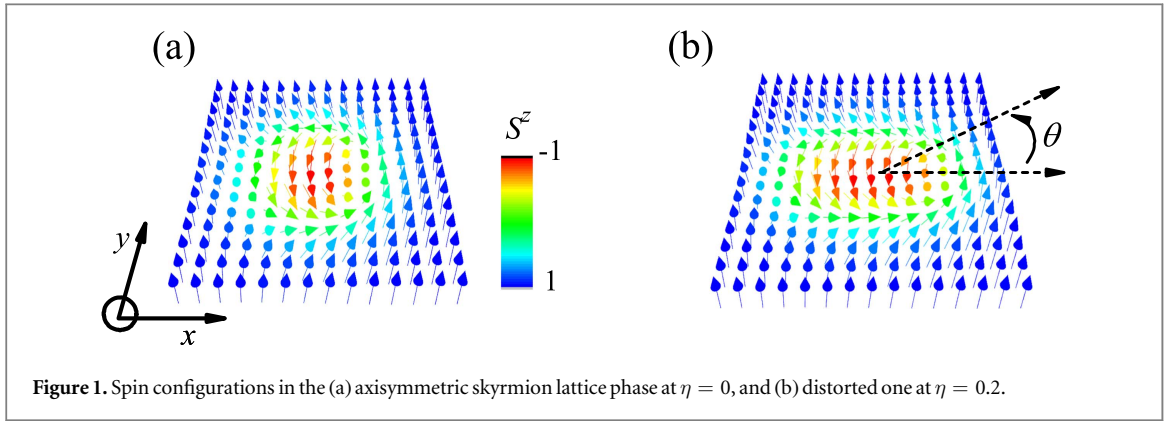**E-mail:** qinmh@scnu.edu.cn and sdong@seu.edu.cn

## Abstract

In this work, we study the microscopic dynamics of distorted skyrmions in strained chiral magnets (Shibatak *et al* 2015 *Nat. Nanotechnol.* **10** 589) under gradient magnetic field and electric current by Landau–Lifshitz–Gilbert simulations of the anisotropic spin model. It is observed that the dynamical responses are also anisotropic, and the velocity of the distorted skyrmion is periodically dependent on the directions of the external stimuli. Furthermore, in addition to the uniform motion, our work also demonstrates an anti-phase harmonic vibration of the two skyrmions in nanostripes, and the frequencies can be effectively modulated by the anisotropic Dzyaloshinskii–Moriya interaction. The simulated results are well explained by Thiele's theory, which may provide useful information in understanding the dynamics of the distorted skyrmions.

## 1. Introduction

A skyrmion is a vortex-like topological spin structure where the spins point in all directions wrapping a sphere, as schematically shown in figure 1(a). It has been observed experimentally in chiral magnets such as MnSi and FeGe, and attracts continuous attentions due to its interesting physics and potential applications for novel data storage devices [1–7]. In these materials, the skyrmions are stabilized by the competition of the Dzyaloshinskii–Moriya (DM) interaction and the ferromagnetic (FM) exchange interaction in the presence of an external magnetic field ($h$), as revealed in earlier works [8–10]. Importantly, it can be well controlled by an ultralow current density of a few $10^2$ A cm$^2$ which is several orders of magnitude smaller than that for magnetic domain walls. Thus, skyrmions were proposed to be promising candidates for high-density and low power consumption magnetic memories, especially considering their inherent topological stability and small lateral size. Moreover, the universal current–velocity relation of the skyrmion motion independent on impurities in chiral magnets was uncovered theoretically [11] and confirmed in the most recent experiments [12].

In addition, effective control of skyrmions has been also demonstrated using other external stimuli such as gradient magnetic/electric field and uniaxial stress [13–16]. For example, a magnetic field gradient $\nabla h$ can drive a Hall-like motion of skyrmions [17–19]. Specifically, the main velocity $v_\perp$ (perpendicular to $\nabla h$) is induced by the gradient, and the low velocity $v_{||}$ (parallel to $\nabla h$) is induced by the damping effect. Furthermore, significant effects of uniaxial strain on the magnetic orders in chiral magnets MnSi and FeGe have been clearly uncovered in experiments [20–22]. It is demonstrated that the uniaxial pressure can significantly modulate the temperature-region of the skyrmion lattice phase in MnSi and can tune the wave vector of the helical order at zero $h$ [20, 23]. Our numerical calculations of the anisotropic spin model suggest that the interaction anisotropies induced by the applied uniaxial stress play an essential role in modulating the magnetic orders [24]. More interestingly, recent experiment demonstrates that even a small anisotropic strain ($\sim$0.3%) in FeGe could induce a large deformation ($\sim$20%) of the skyrmion (as depicted in figure 1(b)) [25]. It is suggested theoretically that the magnitude of the DM interaction is prominently modulated by the lattice distortion, resulting in the

**Figure 1.** Spin configurations in the (a) axisymmetric skyrmion lattice phase at $\eta = 0$, and (b) distorted one at $\eta = 0.2$.

deformation of the skyrmion. Furthermore, distorted skyrmion is suggested to be stabilized in thin films of chiral magnets under tilted magnetic fields and/or with anisotropic environments [26, 27].

While the deformed skyrmions are progressively uncovered, studies proceed in dynamic control of them. The study becomes very important from the following two viewpoints. On one hand, comparing with the axisymmetric skyrmion of which the dynamic response is isotropic, deformed skyrmion could be with a strikingly different response [26]. For example, recent numerically simulations demonstrate that in the presence of the anisotropic DM interaction, the skyrmion/antiskyrmion Hall angle strongly depends on the current direction, suggesting a new degree of freedom to manipulate skyrmions [28]. One may question that if similar anisotropic response of distorted skyrmion to other external stimuli such as gradient magnetic field is also available. The question is vital because the magnetic field manipulation can work for insulators, while the electric current only works for conductors. On the other hand, this study also helps one to understand the interaction between skyrmions which is important in modulating their arrangement and dynamics [29–31]. Generally speaking, repulsive potential between skyrmions in a system makes them to be isolated [29, 32]. Interestingly, it was reported in recent work that skyrmion clusters could be formed in the helical phase of $Cu_2OSeO_3$ due to the attractive skyrmion–skyrmion interactions [33]. Thus, the effects of the interaction between distorted skyrmions on their dynamics deserve to be investigated in order to further understand the microscopic dynamics in strained chiral magnets.

In this work, we numerically study the dynamics of distorted skyrmions in chiral magnets, and demonstrate anisotropic dynamic responses to gradient magnetic field and electric current. Furthermore, in addition to the uniform motion, anti-phase harmonic vibrations of the two skyrmions in nanostripe are uncovered, and the oscillation frequency is mainly determined by the spin configurations of the skyrmions which can be tuned by applied uniaxial strain. The simulated results are well explained by Thiele's theory.

## 2. Model and methods

Following the earlier works [9, 34], we study the classical Heisenberg model on the two-dimensional square lattice for strained chiral magnets, and the Hamiltonian is given by

$$H = -J\sum_{\mathbf{i}}(\mathbf{S_i} \cdot \mathbf{S_{i+\hat{x}}} + \mathbf{S_i} \cdot \mathbf{S_{i+\hat{y}}}) - \sum_{\mathbf{i}}(D_x\mathbf{S_i} \times \mathbf{S_{i+\hat{x}}} \cdot \hat{x} + D_y\mathbf{S_i} \times \mathbf{S_{i+\hat{y}}} \cdot \hat{y}) - \sum_{\mathbf{i}}hS_{\mathbf{i}}^z, \qquad (1)$$

where $\mathbf{S_i}$ is the classical Heisenberg spin with unit length on site $\mathbf{i}$, $\hat{x}$, $\hat{y}$ are the basis vectors of the square lattice. The first term is the isotropic FM exchange interaction between the nearest neighbors with $J = 1$. The second term is the anisotropic DM interaction with a fixed $D_x = 0.5$, and the magnitude of the DM interaction anisotropy is defined by $\eta = D_y/D_x - 1$. The last term is the Zeeman coupling with $h$ applied along the [001] direction. It has been experimentally reported that strain hardly affects the FM exchange interaction in FeGe. In addition, the anisotropy of the FM interaction is expected to affect the deformation of skyrmion similar to the anisotropy of the DM interaction, which is not considered in this work for simplicity.

We investigate the spin dynamics at zero temperature ($T$) by numerically solving the Landau–Lifshitz–Gilbert (LLG) equation:

$$\frac{d\mathbf{S_i}}{dt} = -\gamma\mathbf{S_i} \times \mathbf{f_i} + \alpha\mathbf{S_i} \times \frac{d\mathbf{S_i}}{dt}, \qquad (2)$$

with the local effective field $\mathbf{f_i} = -(\partial H/\partial \mathbf{S_i})$. Here, $\gamma$ is the gyromagnetic ratio, $\alpha$ is the Gilbert damping coefficient. In this work, unless stated elsewhere, $\gamma = 1$ and $\alpha = 0.2$ are selected in reduced units, and the physical conclusion will not be affected by the values of these parameters. When a spin-polarized current is

considered, the LLG equation updates to

$$\frac{dS_i}{dt} = -\gamma S_i \times f_i + \alpha S_i \times \frac{dS_i}{dt} + (j \cdot \nabla)S_i - \beta S_i \times (j \cdot \nabla)S_i. \tag{3}$$

The third term in the right side is the adiabatic spin-transfer-torque term describing the coupling between the spin-polarized current $\mathbf{j}$ ($v_s \sim \mathbf{j}$ is the velocity of the conduction electrons) and localized spins, and the last $\beta$ term is the coupling owing to non-adiabatic effects.

We use the fourth-order Runge–Kutta method to solve the LLG equation. The initial spin configurations are obtained by the Monte Carlo simulations using the over-relaxation algorithm and temperature exchange method. Then, the configurations are sufficiently relaxed by solving the LLG equation. The simulation is performed on an $18 \times 18$ ($16 \times 40$) square lattice to simulate isolated (multiple) skyrmions. Furthermore, we constrain the spin at the edges by $S^z = 1$ to reduce the finite lattice size effect for the case of isolated skyrmions [35], while apply the periodic/free boundary condition along the direction perpendicular to/parallel to the field gradient for the case of multiple skyrmions. The finite-size effect is occasionally checked by the simulation on a $100 \times 100$ system size, which is confirmed to hardly affect our main conclusion. Subsequently, the spin dynamics are investigated under gradient fields, and the simulated results are further explained using the approach proposed by Thiele. Furthermore, the electric current driven motion of isolated skyrmions is also investigated with the periodic boundary condition is applied. The displacement of the skyrmion is characterized by the position of its center $\mathbf{R}$: $\mathbf{R} = \Sigma_r (S^z - 1)r / \Sigma_r (S^z - 1)$ with $r$ is the coordinate of a local spin. Then, the velocity is numerically calculated by $\mathbf{v} = d\mathbf{R}/dt$.

## 3. Results and discussion

Figures 1(a) and (b) give the initial spin configurations of single skyrmions under $h = 0.18$ at $\eta = 0$ and $\eta = 0.2$, respectively. The skyrmion with arbitrary rotation symmetry under isotropic condition ($\eta = 0$) is significantly distorted when the anisotropy of the DM interaction is introduced to simulate anisotropic condition caused by applied strain. Then, the motion of the skyrmion driven by gradient magnetic fields and electric currents with various directions (denoted by the angle $\theta$, as shown in figure 1(b)) are studied in detail.

First, we investigate the gradient-field-driven motion of single distorted skyrmion. Here, the gradient field $\nabla h$ is selected to be small enough (ranged from 0.0001 to 0.0002) to prevent destabilizing the skyrmion. The calculated $v_{\parallel}$ and $v_{\perp}$ of the skyrmions as functions of $\nabla h$ for various $\theta$ at $\eta = 0.16$ are shown in figures 2(a) and (b), respectively. Both $v_{\parallel}$ and $v_{\perp}$ increase linearly with $\nabla h$, the same as the earlier report. Furthermore, for fixed $\nabla h$ and $\theta$, $v_{\perp}$ is rather larger than $v_{\parallel}$, exhibiting a Hall-like motion behavior. Interestingly, $v_{\parallel}$ and $v_{\perp}$ are also dependent on $\theta$ for a fixed $\nabla h$, demonstrating an anisotropic dynamics. Subsequently, the effects of the DM interaction anisotropy on the spin dynamics are investigated. Figure 2(c) shows the simulated $v_{\parallel}$ as a function of $\theta$ for various $\eta$. The $v_{\parallel}/\nabla h$–$\theta$ curves are cosine curves with the period of $\pi$. Furthermore, the amplitude of the curve gradually increases with the increase of $\eta$. The simulated $v_{\perp}/\nabla h$–$\theta$ curves for various $\eta$ are shown in figure 2(d) which clearly demonstrates that $v_{\perp}$ is sinusoidal related with $2\theta$. Moreover, the curve significantly shifts toward the high $v_{\perp}$ side as $\nabla h$ increases.

As a matter of fact, the simulated results can be well explained by Thiele's theory. In the continuum limit, the model Hamiltonian is updated to

$$H = \int \left[ \frac{J}{2}(\nabla S)^2 - D_x(S^y \partial_x S^z - S^z \partial_x S^y) - D_y(S^z \partial_y S^x - S^x \partial_y S^z) - hS^z \right] d^2r, \tag{4}$$
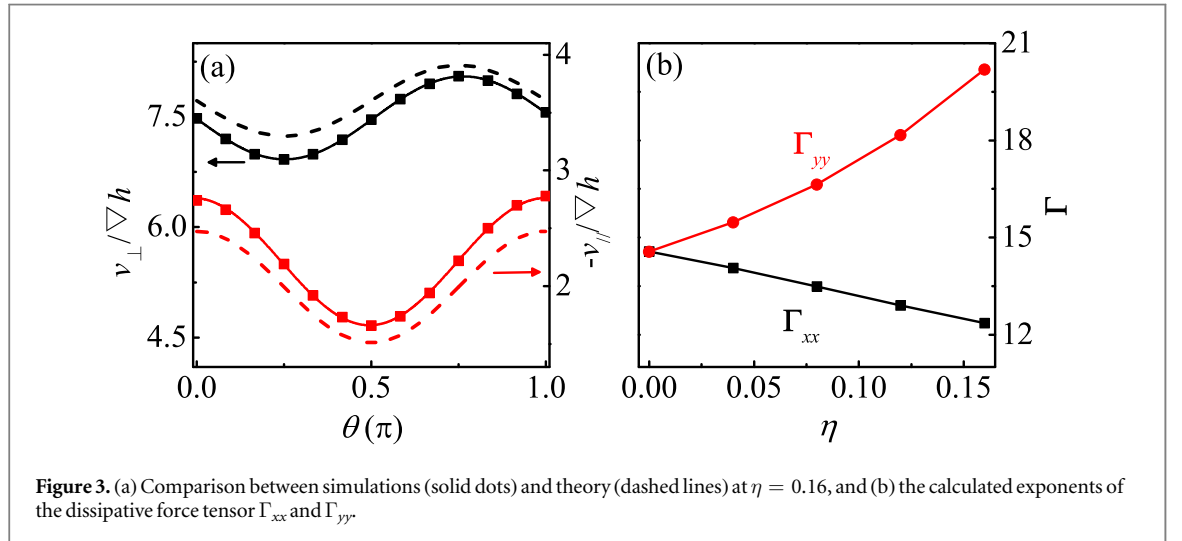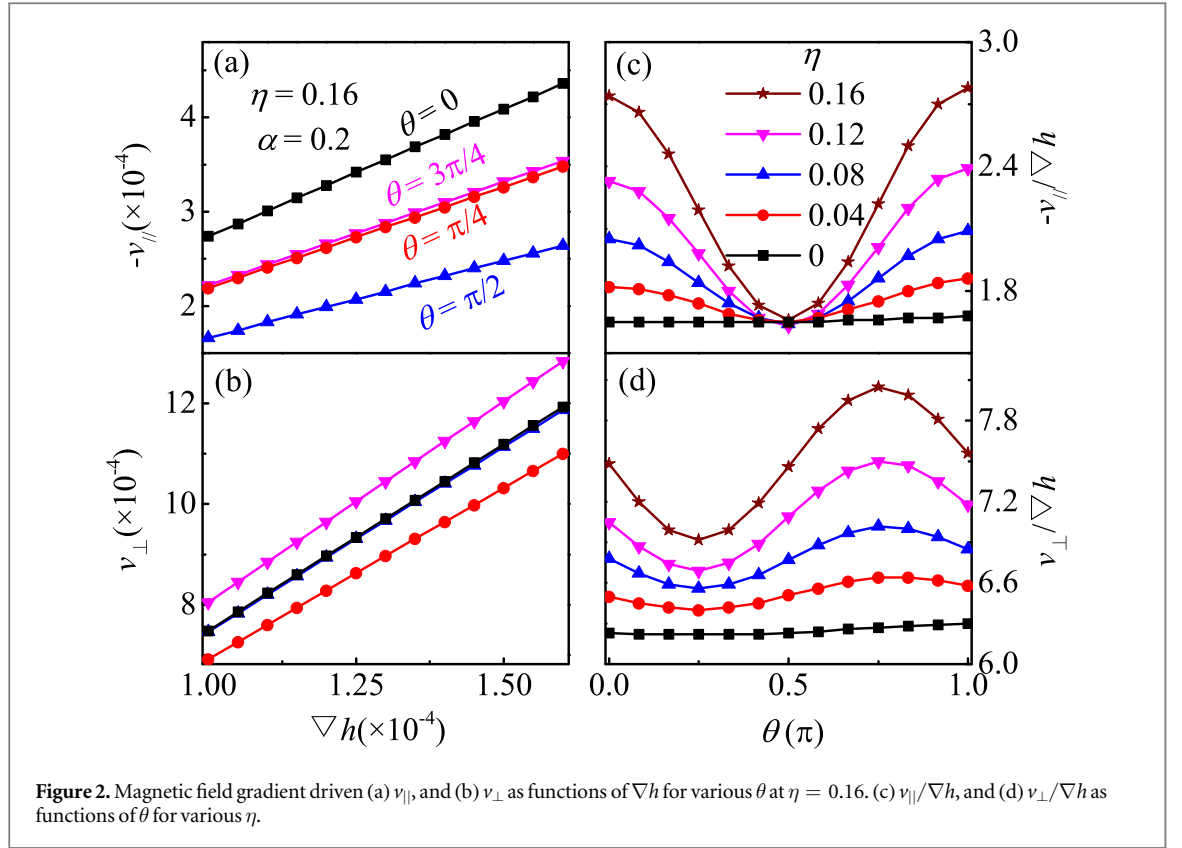
where $S^\mu$ is the $\mu$ ($\mu = x, y, z$) component of the spin. According to the approach proposed by Thiele, one obtains

$$\Gamma(\alpha \mathbf{v} - \beta \mathbf{v}_s) + N_{sk}\hat{\mathbf{z}} \times (\mathbf{v} - \beta \mathbf{v}_s) = -\gamma \frac{\partial H_{sk}}{\partial \mathbf{R}}, \tag{5}$$

where $N_{sk} = 4\pi q$ with $q = 1$ is the topological charge which is not changed for distorted skyrmion, $H_{sk}$ is the energy of the skyrmion. The components of the dissipative force tensor $\Gamma$ is given by

$$\Gamma_{ij} = \int d^2r (\partial_i S \cdot \partial_j S), \tag{6}$$

here, $\Gamma_{xy} = \Gamma_{yx} = 0$ is obtained even for distorted skyrmion due to its $\pi$-rotation symmetry. Subsequently, the velocity of the distorted skyrmion under the gradient field can be calculated by

**Figure 2.** Magnetic field gradient driven (a) $v_\parallel$, and (b) $v_\perp$ as functions of $\nabla h$ for various $\theta$ at $\eta = 0.16$. (c) $v_\parallel / \nabla h$, and (d) $v_\perp / \nabla h$ as functions of $\theta$ for various $\eta$.



**Figure 3.** (a) Comparison between simulations (solid dots) and theory (dashed lines) at $\eta = 0.16$, and (b) the calculated exponents of the dissipative force tensor $\Gamma_{xx}$ and $\Gamma_{yy}$.

$$\begin{cases} v_\parallel = \dfrac{\alpha[(\Gamma_{yy} - \Gamma_{xx})\sin^2\theta - \Gamma_{yy}]}{\alpha\alpha\Gamma_{xx}\Gamma_{yy} + N_{sk}^2}\gamma\dfrac{\partial H_{sk}}{\partial \mathbf{R}} \\[2mm] v_\perp = \dfrac{2N_{sk} - (\Gamma_{yy} - \Gamma_{xx})\alpha\,\sin 2\theta}{2(\Gamma_{yy}\Gamma_{xx}\alpha\alpha + N_{sk}^2)}\gamma\hat{\mathbf{z}} \times \dfrac{\partial H_{sk}}{\partial \mathbf{R}}, \end{cases} \tag{7}$$

where $\partial H_{sk}/\partial \mathbf{R} = Q\nabla h$ with the magnetic charge $Q = \Sigma_i[1 - S_i^z]$. It is easily noted that for a fixed $h$, noncollinear spin structures are favored and $\Sigma_i S_i^z$ is decreased when the DM interaction is enhanced. Thus, $Q$ increases as $\eta$ increases, resulting in the increase of the velocity. Figure 3(a) shows the theoretical $v_\perp / \nabla h$–$\theta$ and $v_\parallel / \nabla h$–$\theta$ curves (dashed lines) and the corresponding simulated curves (solid dots) at $\eta = 0.16$. The theoretical result coincides well with the simulated one (the discrepancy of $v_\perp$ is less than 5%), further confirming our simulations. It is noted that Thiele approach investigates the continuum limit of the model, while the LLG simulation studies the discrete model, mainly contributing to the systematic discrepancy. Obviously, equation (7) demonstrates that the velocity is independent on $\theta$ for $\Gamma_{yy} = \Gamma_{xx}$ which is available at $\eta = 0$. Furthermore, the value of $(\Gamma_{yy} - \Gamma_{xx})$ quickly increases with the increasing $\eta$, as clearly shown in figure 3(b).

**Figure 4.** Electric current driven (a) $v_{||}/v_s$ and (b) $v_{\perp}/v_s$ as functions of $\theta$ at $\beta = 0.1$ for various $\eta$. (c) $v_{||}/v_s$ and (d) $v_{\perp}/v_s$ as functions of $\theta$ for various $\beta$.
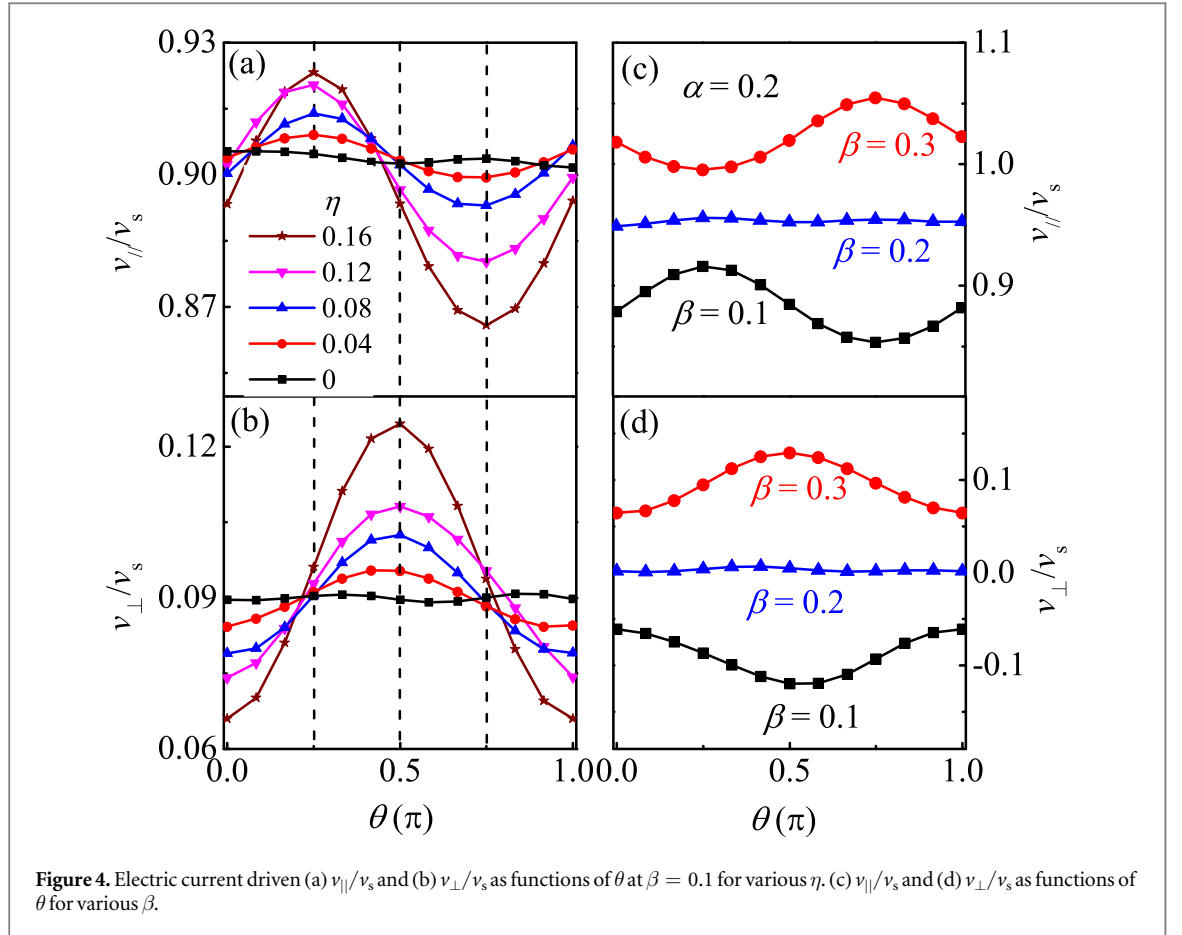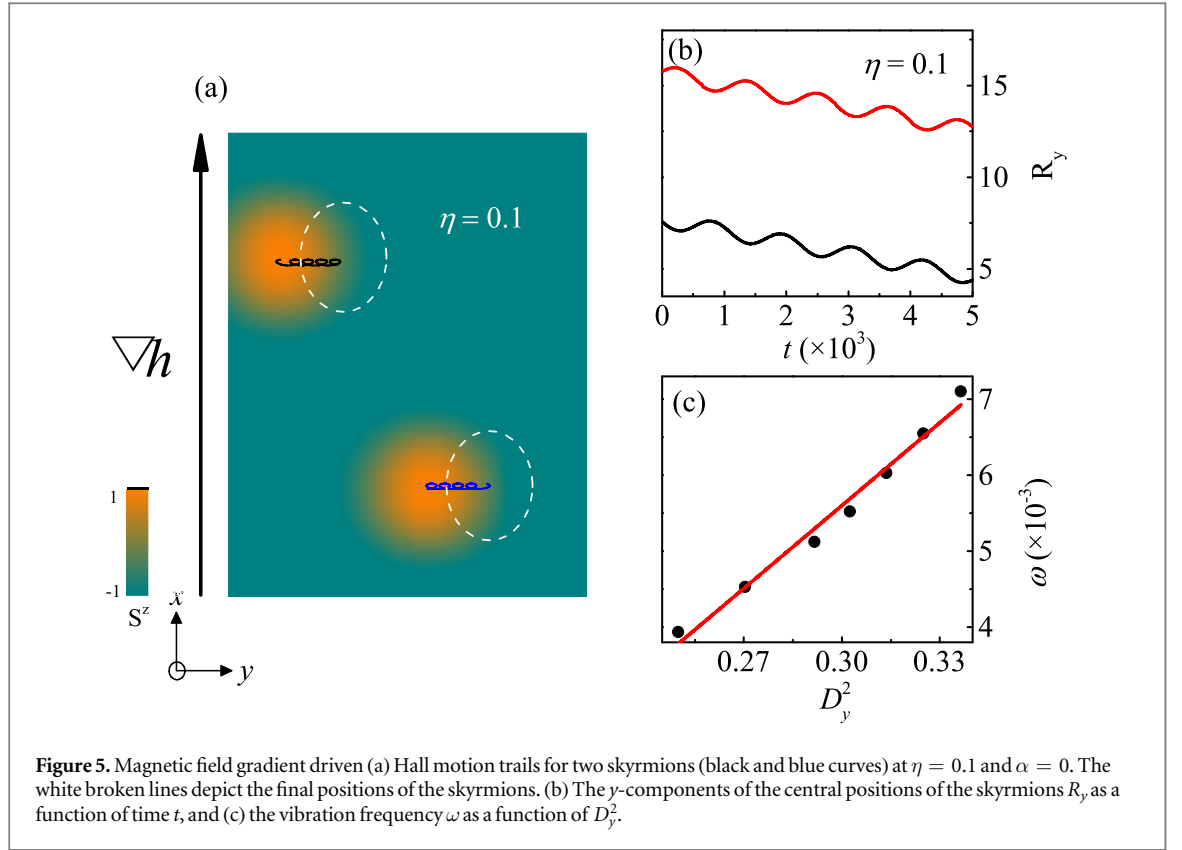
Thus, the magnitude of the dynamics anisotropy (qualitatively denoted by the amplitude of the periodic modulation) is significantly increased, as revealed in our simulations. Moreover, for a fixed $\eta$, the amplitude of the curve is linearly dependent on $\alpha$, which has been confirmed in our simulations, although the corresponding results are not shown here.

For integrity, we also investigate the current driven single distorted skyrmion motion. Based on the Thiele's theory, the velocities are given by

$$
\begin{cases}
v_{||} = \dfrac{(\Gamma_{yy} - \Gamma_{xx})(\alpha - \beta)N_{sk}\sin 2\theta - 2(\Gamma_{yy}\Gamma_{xx}\alpha\beta + N_{sk}^2)}{2(\Gamma_{yy}\Gamma_{xx}\alpha\alpha + N_{sk}^2)}v_s \\[3mm]
v_{\perp} = \dfrac{(\alpha - \beta)N_{sk}[(\Gamma_{yy} - \Gamma_{xx})\sin^2\theta + \Gamma_{xx}]}{\Gamma_{yy}\Gamma_{xx}\alpha\alpha + N_{sk}^2}(\hat{z} \times \boldsymbol{v}_s).
\end{cases}
\tag{8}
$$

It is clearly demonstrated that the spin response to the current is anisotropic (both $v_{||}$ and $v_{\perp}$ are periodically modulated by $2\theta$), and the magnitude of the response anisotropy is linearly related with $(\alpha - \beta)(\Gamma_{yy} - \Gamma_{xx})$. Figures 4(a) and (b) show the LLG simulated $v_{||}$ and $v_{\perp}$ as functions of $\theta$ for various $\eta$ at $\beta = 0.1$. It is noted that $(\Gamma_{yy} - \Gamma_{xx})$ quickly increases with the increasing $\eta$, resulting in the enhancement of the response anisotropy. Furthermore, for $\alpha = \beta$, $v_{||}$ and $v_{\perp}$ are independent on $\theta$, as clearly shown in figures 4(c) and (d) which give the simulated results for various $\beta$ at $\eta = 0.16$. More importantly, the transverse motion of the skyrmion is eliminated, and the skyrmion propagates along the current direction with zero Hall motion. Thus, one may choose particular materials and apply external stimuli along particular directions to reduce $v_{||}$ or $v_{\perp}$, and in turn to better control the motion of the skyrmions.

At last, we study the gradient-field-driven motions of multi-skyrmions in chiral nanostripes and pay particular attention to the effect of the skyrmion–skyrmion interaction. For simplicity, the width of the nanostripe is reasonably selected to stabilize only two skyrmions as depicted in figure 5(a). Furthermore, $\alpha = 0$ is chosen for this case, and only Hall motions of the skyrmions are available. This conveniently allows us to focus on the effect of the skyrmion–skyrmion interaction. Figure 5(b) gives the time-dependent $y$-components of the position-centers of the skyrmions at $\eta = 0.1$. It is clearly shown that the skyrmions propagate in a longitudinal-wave-like way. For a fixed $\eta$, the motion of each skyrmion could be decomposed into a uniform motion and a

**Figure 5.** Magnetic field gradient driven (a) Hall motion trails for two skyrmions (black and blue curves) at $\eta = 0.1$ and $\alpha = 0$. The white broken lines depict the final positions of the skyrmions. (b) The $y$-components of the central positions of the skyrmions $R_y$ as a function of time $t$, and (c) the vibration frequency $\omega$ as a function of $D_y^2$.

simple harmonic vibration. Furthermore, the two harmonic vibrations can be described as $v' = A\sin(\omega t + \varphi)$ with a same frequency $\omega$, a same amplitude $A$ and a fixed phase difference of $\pi$.

Moreover, it is clearly shown that $\omega$ is mainly dependent on the value of the DM interaction $D_y$ (figure 5(c)), and is hardly related to the magnitude of the field gradient. Thus, it is strongly suggested that $\omega$ may be the eigenfrequency determined by the configuration of the skyrmion which is modulated by the DM interaction. In other words, the skyrmion–skyrmion interaction is mainly determined by the DM interaction anisotropy, which tunes the vibration mode of the skyrmions. As an approximation, the energy transfer between the FM exchange and DM interactions $\Delta E$ depending on the displacement of the skyrmion from the equilibrium position $\Delta R_y$ can be estimated by expanding the energy nearing the equilibrium wave vector $k_y = \tan(D_y/J)$,

$$\Delta E = \frac{JD_y \tan^3(D_y/J)}{2\pi\sqrt{J^2 + D_y^2}}(\Delta R_y)^2. \qquad (9)$$

Subsequently, the frequency $\omega$ could be calculated by $\omega \sim g^{1/2}$ with the so-called elastic coefficient $g$

$$g = \frac{JD_y \tan^3(D_y/J)}{2\pi\sqrt{J^2 + D_y^2}}. \qquad (10)$$

As a result, the frequency $\omega \sim (D_y)^2$ can be obtained, as confirmed in our simulated results in figure 5(c) which gives the simulated $\omega$ as a function of $D_y^2$. As a matter of fact, the fixed $\pi$ phase difference between the two vibrations can also be explained by Thiele's theory. Regarding the two skyrmions as a whole, the skyrmion–skyrmion interaction potential is independent of their central location. Thus, the average velocity of the two skyrmions will not be changed for a fixed DM interaction, resulting in the anti-phase vibrations. Furthermore, the wave vector of one of the helical orders significantly increases as $D_y$ increases, resulting in the increases of the repulsive potential between the skyrmions and of $\omega$, as demonstrated in our simulations. Moreover, $\omega$ is less relevant to $D_x$, which has been confirmed in our simulations (although the corresponding results are not shown here for brevity), further demonstrating that the above analysis is reasonable. In addition, a nonzero $\alpha$ gradually diminishes the amplitude of the oscillation, and hardly changes the oscillation frequency.

Up to now, experimental knowledge of the microscopic dynamics of distorted skyrmions in strained chiral magnets remains ambiguous. Interestingly, this work clearly demonstrates that distorted skyrmions exhibit anisotropic responses depending on the directions of the field gradient or applied electric current. In real materials, one may choose particular directions of external stimuli to reduce perpendicular/parallel drift velocity in order to better control the motion of the skyrmions. Moreover, in addition to the uniform motion,

the anti-phase vibrations of the two skyrmions are observed, and the vibration frequency is mainly determined by the spin configurations of the skyrmions which can be modulated by applied strain. This phenomenon may provide useful information for future device design.

## 4. Conclusion

In conclusion, we have studied the dynamics of the distorted skyrmions in chiral magnets based on the LLG simulations of the anisotropic spin model. It is demonstrated that the velocities of the skyrmions are significantly dependent on the directions of the magnetic field gradient or the electric current, exhibiting the behavior of the anisotropic dynamics control. Furthermore, in addition to the uniform motion, the anti-phase harmonic vibrations of the two skyrmions in chiral nanostripes are observed, and whose frequency is mainly determined by the spin configurations which can be modulated by applied strain. The simulated results are well explained by Thiele's theory and are meaningful in understanding the dynamics of the distorted skyrmions.

## Acknowledgments

## ORCID iDs

M Zeng ⓘ https://orcid.org/0000-0003-3594-7619
S Dong ⓘ https://orcid.org/0000-0002-6910-6319

## References

[1] Mühlbauer S, Binz B, Jonietz F, Pfleiderer C, Rosch A, Neubauer A, Georgii R and Böni P 2009 *Science* **323** 915
[2] Neubauer A, Pfleiderer C, Binz B, Rosch A, Ritz R, Niklowitz P G and Böni P 2009 *Phys. Rev. Lett.* **102** 186602
[3] Jonietz F *et al* 2010 *Science* **330** 1648
[4] Yu X Z, Onose Y, Kanazawa N, Park J H, Han J H, Matsui Y, Nagaosa N and Tokura Y 2010 *Nature* **465** 901
[5] Yu X Z, Kanazawa N, Onose Y, Kimoto K, Zhang W Z, Ishiwata S, Matsui Y and Tokura Y 2011 *Nat. Mater.* **10** 106
[6] Wilhelm H, Baenitz M, Schmidt M, Rößler U K, Leonov A A and Bogdanov A N 2011 *Phys. Rev. Lett.* **107** 127203
[7] Seki S, Yu X Z, Ishiwata S and Tokura Y 2012 *Science* **336** 198
[8] Bak P and Jensen M H 1980 *J. Phys. C: Solid State Phys.* **13** L881
[9] Yi S D, Onoda S, Nagaosa N and Han J H 2009 *Phys. Rev.* B **80** 054416
[10] Park J H and Han J H 2011 *Phys. Rev.* B **83** 184406
[11] Iwasaki J, Mochizuki M and Nagaosa N 2013 *Nat. Commun.* **4** 1463
[12] Legrand W, Maccariello D, Reyren N, Garcia K, Moutafis C, Luchaire C, Collin S, Bouzehouane K, Cros V and Fert A 2017 *Nano Lett.* **17** 2703
[13] Sampaio J, Cros V, Rohart S, Thiaville A and Fert A 2013 *Nat. Nanotechnol.* **8** 839
[14] Mochizuki M 2012 *Phys. Rev. Lett.* **108** 017601
[15] Liu Y H, Li Y Q and Han J H 2013 *Phys. Rev.* B **87** 100402
[16] Koshibae W, Kaneko Y, Iwasaki J, Kawasaki M, Tokura Y and Nagaosa N 2015 *Jpn. J. Appl. Phys.* **54** 053001
[17] Everschor K, Garst M, Binz B, Jonietz F, Mühlbauer S, Pfleiderer C and Rosch A 2012 *Phys. Rev.* B **86** 054432
[18] Komineas S and Papanicolaou N 2015 *Phys. Rev.* B **92** 064412
[19] Wang C J, Xiao D, Chen X, Zhou Y and Liu Y W 2017 *New J. Phys.* **19** 083008
[20] Chacon A, Bauer A, Adams T, Rucker F, Brandl G, Georgii R, Garst M and Pfleiderer C 2015 *Phys. Rev. Lett.* **115** 267202
[21] Butenko A B, Leonov A A, Rößler U K and Bogdanov A N 2010 *Phys. Rev.* B **82** 052403
[22] Wilson B N, Butenko A B, Bogdanov A N and Monchesky T L 2014 *Phys. Rev.* B **89** 094411
[23] Nii Y, Nakajima T, Kikkawa A, Yamasaki Y, Ohishi K, Suzuki J, Taguchi Y, Arima T, Tokura Y and Iwasa Y 2015 *Nat. Commun.* **6** 8539
[24] Chen J, Cai W P, Qin M H, Dong S, Lu X B, Gao X S and Liu J M 2017 *Sci. Rep.* **7** 7392
[25] Shibata K *et al* 2015 *Nat. Nanotechnol.* **10** 589
[26] Lin S Z and Saxena A 2015 *Phys. Rev.* B **92** 180401
[27] Hagemeister J, Vedmedenko E Y and Wiesendanger R 2016 *Phys. Rev.* B **94** 104434
[28] Huang S Y, Zhou C, Chen G, Shen H Y, Schmid A K, Liu K and Wu Y Z 2017 *Phys. Rev.* B **96** 144412
[29] Bogdanov A 1995 *JETP Lett.* **62** 247
[30] Lin S-Z, Reichhardt C, Batista C D and Saxena A 2013 *Phys. Rev.* B **87** 214419
[31] Zhang X C, Zhao G P, Fangohr H, Liu J P, Xia W X, Xia J and Morvan F J 2015 *Sci. Rep.* **5** 7643
[32] Zhang X, Zhao G, Fangohr H, Liu J P, Xia W, Xia J and Morvan F 2015 *Sci. Rep.* **5** 7643
[33] Müller J, Rajeswari J, Huang P, Murooka Y, Rønnow H M, Carbone F and Rosch A 2017 *Phys. Rev. Lett.* **119** 137201

[34] Buhrandt S and Fritz L 2013 *Phys. Rev.* B **88** 195137
[35] Liang J J, Yu J H, Chen J, Qin M H, Zeng M, Lu X B, Gao X S and Liu J-M 2018 *New J. Phys.* **20** 053037